The bound $\mu^+\mu^-$ system

U. D. Jentschura *, G. Soff
Institut für Theoretische Physik, TU Dresden, 01062 Dresden, Germany

V. G. Ivanov
Pulkovo Observatory, 196140, St. Petersburg, Russia

S. G. Karshenboim†
D. I. Mendeleev Institute for Metrology, 198005, St. Petersburg, Russia,
Max–Planck–Institut für Physik komplexer Systeme, Bayreuther Straße 40, 01069 Dresden, Germany

We consider the hyperfine structure, the atomic spectrum and the decay channels of the bound $\mu^+\mu^-$ system (dimuonium). The annihilation lifetimes of low-lying atomic states of the system lie in the 10^{-12} s range. The decay rates could be measured by detection of the decay products (high energy photons or electron-positron pairs). The hyperfine structure splitting of the dimuonic system and its decay rate are influenced by electronic vacuum polarization effects in the far time-like asymptotic region. This constitutes a previously unexplored kinematic regime. We evaluate next–to–leading order radiative corrections to the decay rate of low-lying atomic states. We also obtain order $\alpha^5\, m_\mu$ corrections to the hyperfine splitting of the $1S$ and $2S$ levels.

I. INTRODUCTION

The bound system consisting of two muons (dimuonium) can be produced in heavy nuclei inelastic scattering at high energies and in particle decays. The decay of the neutral η^0 meson into dimuonium has been investigated theoretically by L. Nemenov [1] ($\eta^0 \to \mathit{dimuonium} + \gamma$). The formation of dimuonium in pion–proton collisions ($\pi^- + p \to \mathit{dimuonium} + n$) and by photons on nuclei ($\gamma + Z \to \mathit{dimuonium} + Z$) has been discussed in [2]. For the direct production of dimuonium in muon–antimuon collisions, considerable experimental difficulties associated with slow muon beams would have to be overcome. Another possible pathway for the production of the system, which we do not discuss in any further detail here, is the e^+e^--annihilation (near or above the μ threshold). Dimuonium, once produced, undergoes atomic decay (into energetically lower atomic states) and annihilation decay (into electrons and photons). Because the annihilation products are hard photons and relativistic electron–positron pairs, the decays could be investigated experimentally by established methods of particle physics.

In this work, we devote special attention to the annihilation decay rates of low-lying atomic states. The decay rate of the $S = 1$ ortho states of dimuonium has been evaluated by J. Malenfant in pioneering investigations [3,4]. The name "dimuonium" has been proposed in [4]. This work can therefore be regarded as a continuation of the earlier investigations on the system. We try to refine the analysis of the ortho–states, and we investigate in addition the $S = 0$ para states. We obtain corrections to the decay rate in next–to–leading order.

In this work, we also investigate the hyperfine structure in next–to–leading order. We further discuss briefly the atomic spectrum of dimuonium. The contribution of electronic vacuum polarization to the hyperfine structure and to the decay rate of ortho states lies in the far time-like asymptotic region. Its observation would constitute a test of QED in this previously unexplored kinematic regime. Due to the small length scale of the system, the hyperfine structure of the dimuonic atom is influenced by the effect of hadronic vacuum polarization (at the level of one part in 10^3).

Among the exotic atomic systems, some attention has recently been devoted to pionium ($\pi^+\pi^-$-system). The spectrum and decay channels of pionium have been discussed extensively (see e. g. [5–7]). The production of pionium has been observed recently [8]. The formation of bound atomic systems in particle decays has been observed earlier. Positronium has been detected in the decay $\pi^0 \to \mathrm{Ps} + \gamma$ [9]. The bound system of a pion and a muon ($\pi\mu$) has been observed in the decay $K_L^0 \to (\pi\mu\,\mathrm{atom}) + \nu$ [10].

*Electronic address: ulj@nist.gov
†Electronic address: sgk@onti.vniim.spb.su

In contrast to the short–lived $\pi^+\pi^-$ system, where $c \cdot \tau$ is in the range of $1\,\mu$m, $c \cdot \tau$ is in the range of 1 mm for dimuonium, so that the atom could leave the beam target after production. In any of the cases discussed the production rate is expected to be proportional to the atomic wave function at the origin $|\psi_{nl}(0)|^2 = \alpha^3\, m_\mu^3\, \delta_{l0}/[8\,\pi\, n^3]$ (we use relativistic units in which $\hbar = c = 1$ and $\alpha = e^2$). Hence only low-lying states with zero orbital moment (S states) are expected to be produced.

This paper is organized as follows. We first study the spectrum of the system including radiative corrections (Lamb shift, Section II). We then proceed to an investigation of the hyperfine structure in Section III. As the highest accuracy can presumably be obtained in decay rate measurements, we devote special attention to the decay channels which are investigated in detail in Sections IV and V.

II. THE ATOMIC SPECTRUM OF DIMUONIUM

The dimuonic atom is an analogue of the hydrogen, muonic hydrogen and positronium atoms. The main feature of muonic hydrogen (μH) which differs from properties of hydrogen is the order of magnitude of the Lamb shift relative to the fine structure splitting (see e. g. [11]). The fs splitting in μH and H (also in positronium and dimuonium) is of the order of $\alpha^4\, m_r$, where m_r denotes the reduced mass of the system, which is roughly equal to the mass of the lighter particle in a system with a heavy nucleus. In hydrogen the Lamb shift of the order of $\alpha^5\, m_r$, whereas in muonic systems, the Lamb shift is of the order of $\alpha^3\, m_r$, because of the large effect of vacuum polarization. The above considerations are parametrically true for all states, but numerical coefficients turn out to be largest for S states. Because the coefficients to the Lamb shift are negative (attractive Uehling potential), S states are significantly lowered in energy in muonic systems. In Fig. 1 we present an overview over the spectrum of hydrogen, μH, positronium and $\mu^+\mu^-$.

In both hydrogen and μH, the hyperfine structure is a smaller effect of order $\alpha^4\,(m_r^2/M)$ (M denotes the mass of the nucleus). This is different in positronium. Positronium has a more complicated spectrum than the hydrogen atom. Due to the larger magnetic moment of the "central" particle (and its smaller mass), and due to virtual pair annihilation processes, the effects which are responsible for the fine and hyperfine structure and for the Lamb shift have the same order of magnitude: $\alpha^4\, m_r$. For positronium as well as for hydrogen, the fine structure is defined as the separation of levels with the same principal and angular orbital momentum quantum numbers.

In positronium, different quantum numbers have to be used for the classification of levels than in an atom with a heavy nucleus. For a system with a heavy nucleus, the total electron moment $\boldsymbol{j} = \boldsymbol{l} + \boldsymbol{s}$ is conserved within the central field approximation. States are classified as $nljF$. In positronium the total spin $\boldsymbol{S} = \boldsymbol{s}_1 + \boldsymbol{s}_2$ is an exactly conserved quantity. States are classifyed as $nlSF$ (denoted as $n^{2\,S+1}l_F$), where $S = 1$ for an ortho and $S = 0$ for para states. In all systems considered we denote the total angular atomic moment by F. Although the atomic spectrum of dimuonium is determined by a large Lamb shift of order $\alpha^3\, m_r$ (as is the case for μH), the classification of levels is like in positronium (quantum numbers $nlSF$).

There exists no close analogy of dimuonium with pionium, because pionium containes only spinless particles, and the spectrum includes neither a fine nor a hyperfine structure. Due to the strong interaction, the hadronic pionium system lives only a very short time, and the atomic structure cannot be investigated (because the decay rate exceeds the rate of atomic transitions). By contrast, for P-states in dimuonium, the atomic transition $nP \to n'S$ ($n' < n$) dominates over the annihilation decay rate. The lifetime of the atomic levels is considered in section III.

The main contribution to the Lamb shift in dimuonium is caused by the one–loop electronic vacuum polarization. Due to the small spatial separation of the two muons in the $\mu^+\mu^-$ system, the charge of the two particles, which is larger than the effective charge to be observed at larger distance, is less screened and causes a deviation of the energy levels of the order $\alpha^3\, m_r$. For hydrogen, the vacuum polarization enters at the order of $\alpha^5\, m_r$, but for dimuonium, two powers of α are compensated for by the muon-electron mass ratio (or, by employing a coordinate space picture, by the smaller separation of the particles).

We now turn to a brief discussion of the atomic levels of dimuonium. The effect of electronic vacuum polarization on the spectrum is investigated. Any vacuum polarization insertion in the photon line can be represented as a substitution of the form

$$\frac{1}{q^2 + i\,\epsilon} \to \frac{\alpha}{\pi} \int_{s_0}^{\infty} ds\; \rho(s)\, \frac{1}{q^2 - s + i\,\epsilon} \tag{1}$$

in the photon propagator. The integration has to be performed from the threshold s_0 of pair production of the loop particle. For electronic vacuum polarization, the spectral function is given by (see for instance [12], p. 323)

$$\rho(s) = \frac{1}{3\,s} \sqrt{1 - \frac{4\,m_e^2}{s}}\, \left(1 + \frac{2\,m_e^2}{s}\right). \tag{2}$$

The substitution

$$v^2 = 1 - \frac{4\,m_e^2}{s} \tag{3}$$

brings the one-loop vacuum polarization integral into the form [13]

$$\frac{1}{q^2 + i\,\epsilon} \to \frac{\alpha}{\pi} \int_0^1 dv\, \frac{v^2(1 - v^2/3)}{1 - v^2}\, \frac{1}{q^2 - \lambda^2 + i\,\epsilon}\,. \tag{4}$$

For space-like momentum transfer, this can be Fourier-transformed into coordinate space and yields the Uehling potential,

$$V_U(\boldsymbol{r}) = \frac{\alpha}{\pi} \int_0^1 dv\, \frac{v^2(1 - v^2/3)}{1 - v^2}\, \exp\left(-\lambda\, r\right)\, \left[\frac{-\alpha}{r}\right]\,. \tag{5}$$

We have introduced the notation,

$$\lambda = \frac{2\,m_e}{\sqrt{1 - v^2}}\,. \tag{6}$$

The correction to the energy due to the diagram in Fig. 2 is the main contribution to the Lamb shift. The evaluation of the matrix element of the Uehling potential on the non-relativistic wave functions leads to the results listed in Table I. The Rydberg constant for the dimuonic atom is given by

$$E_0 = \frac{\alpha^2\, m_r^2}{2} = \frac{\alpha^2\, m_\mu}{4} = 1406.6133(5)\,\mathrm{eV}, \tag{7}$$

using the recommended values for $\alpha^{-1} = 137.0359895(61)$ and $m_\mu = 105.658389(91)\,\mathrm{MeV}$ [14,15]. The approximate Lamb shift values are (neglecting higher order corrections corrections which are estimated to be suppressed by an additional factor of α/π):

$$\mathcal{L}(1S) = -0.49\,\mathrm{eV}, \quad \mathcal{L}(2S) = -0.058\,\mathrm{eV}, \quad \mathcal{L}(2P) = -0.0014\,\mathrm{eV}. \tag{8}$$

In contrast to muonic hydrogen (μH), dimuonium is a purely leptonic system. Therefore its spectrum is not influenced by nuclear structure effects.

III. HYPERFINE STRUCTURE OF DIMUONIUM

The fine and hyperfine structure in dimuonium and positronium in lowest order $\alpha^4\, m$ are given by the following formula (see for details textbooks [11,12,16] and articles [17–19]),

$$E_{\mathrm{Ps}}(nlSF) = -\frac{\alpha^2}{4\,n^2}\, m + \alpha^4\, m \left[\frac{11}{64\,n^4} + \frac{\delta_{S,1}}{n^3}\, \left(\frac{7}{6}\,\delta_{l,0} + \frac{1 - \delta_{l,0}}{4(2\,l + 1)} B_{j,l}\right) - \frac{1}{2\,n^3\,(2l + 1)}\right], \tag{9}$$

where

$$B_{j,l} = \begin{cases} \frac{3\,l+4}{(l+1)\,(2\,l+3)} & \text{for} \quad F = l + 1, \\ -\frac{1}{l(l+1)} & \text{for} \quad F = l, \\ -\frac{3l-1}{l\,(2\,l-1)} & \text{for} \quad F = l - 1\,. \end{cases} \tag{10}$$

Here m is the mass of the constituent particle, i. e. $m = m_e$ for positronium, $m = m_\mu$ for dimuonium. Note that the above formula determines the position of energy levels in positronium up to the order of α^4. Radiative corrections in Ps enter at the order of α^5, at the order of α^3 in dimuonium. However, for the fine and hyperfine structure of dimuonium in lowest order, the above formula remains valid. The results for the hyperfine structure order in dimuonium in leading order are

$$E^{(0)}_{\rm hfs}(nS) = E_F/n^3, \quad \text{where} \quad E_F = \frac{7}{12}\,\alpha^4\,m_\mu = 0.175\,\text{eV} = 4.23\cdot 10^8\,\text{MHz}\,. \tag{11}$$

The hyperfine structure interval $E^{(0)}_{\rm hfs}(nS)$ arises from the exchange and annihilation diagrams (see Fig. 3), which contribute $4/7\,E_F$ and $3/7\,E_F$ to the Fermi energy E_F, respectively. The triplet n^3S_1 states are energetically higher than the singlet n^1S_0 states. For P states, the α^4 corrections imply the following order of the spectrum, in decreasing energy: n^3P_2, n^1P_1, n^3P_1, n^3P_0 (we follow here the usual spectroscopic notation $n^{2S+1}l_F$).

We now turn to the evaluation of radiative corrections to the hyperfine structure splitting for S states of order $\alpha/\pi\,E_F$ (corresponding to $\alpha/\pi\,E^{(0)}_{\rm hfs}$). Some contributions are the same for positronium and dimuonium, some are specific to the dimuonic system. The contributions which are alike for both systems are depicted in Fig. 4. These contributions originate from the anomalous magnetic moment of the electron in the transverse photon diagram (denoted as "(g-2)-T"), from recoil corrections (denoted by "Rec"), from the vertex correction to the annihilation diagram (denoted by "Vert-A"), from the muonic vacuum polarization ("VP-μ-A"), and from box-diagrams corresponding to two-photon annihilation (denoted by "2A"). In this paper, due to the multitude of corrections considered, we prefer to denote the contributions by short abbreviations, which we hope are self–explanatory, rather then single letters, in order to enhance the clarity of presentation. The results for the above corrections are listed in Table II (first 5 contributions, above the separating line). The sum of corrections to the Fermi energy of order $\alpha/\pi\,E_F$ amounts to [12,20]

$$\Delta E_{\rm Ps}(nS) = \frac{\alpha}{\pi}\left[-\frac{32}{21} - \frac{6}{7}\ln 2 + \frac{3}{7}\,\pi\,i\right]\,\frac{E_F}{n^3}\,, \tag{12}$$

where the imaginary part is entirely due to paradimuonium. It corresponds to the two-photon decay of the para system [18,21]

$$\frac{1}{\Gamma^{(0)}(n^1S_0)} = \tau^{(0)}(n^1S_0) = \frac{2\,n^3}{\alpha^5\,m_\mu} = n^3\cdot 0.6021\cdot 10^{-12}\,\text{s}\,. \tag{13}$$

Now we turn to the evaluation of corrections specific to dimuonium (the relevant diagrams are depicted in Fig. 5). We first evaluate the correction due to vacuum polarization insertions in the Coulomb photon line. For the dimuonic atom, the correction to the wave function due to electronic vacuum polarization has relative order α/π and therefore modifies the hyperfine splitting in α/π relative order. The order of magnitude of this correction is specific to the dimuonic atom (small length scale of the system, see Section I. For "VPC-T" (see Fig. 5), the contribution is given by the matrix element

$$\Delta E_{\rm VPC-T} = 2\times\frac{4}{3}\,\frac{\pi\,\alpha}{m_\mu^2}\,\langle\psi|\delta(\boldsymbol{r})\,\overline{G}(E_\psi)\,V_U|\psi\rangle, \tag{14}$$

where

$$\overline{G}(E_\psi) = \sum_{\psi_n\neq\psi}\frac{|\psi_n\rangle\langle\psi_n|}{E_\psi - E_n} \tag{15}$$

is the reduced Coulomb Green function (the pole of the reference state is excluded from the sum over all intermediate states). Because atomic momenta are of the order of $\alpha\,m_\mu$ in the system under consideration, it is sufficient to carry out the calculations with non–relativistic wave functions. The reduced Green function is a function of two coordinates $\boldsymbol{r}_1$ and $\boldsymbol{r}_2$. Due to the appearance of the δ-like potential the Green function is needed only for $\boldsymbol{r}_1 = \boldsymbol{0}$. It can be expressed in closed form [24],

$$\overline{G}_{1S}(E_{1S};0,\mathbf{r}) = \frac{\alpha m_r^2}{4\pi}\,\frac{2e^{-z_1/2}}{z_1}\Big[2z_1(\ln z_1 + C) + z_1^2 - 5z_1 - 2\Big], \tag{16}$$

and

$$\overline{G}_{2S}(E_{2S};0,\mathbf{r}) = -\frac{\alpha m_r^2}{4\pi}\,\frac{e^{-z_2/2}}{2z_2}\Big[4z_2(z_2-2)(\ln z_2 + C) + z_2^3 - 13z_2^2 + 6z_2 + 4\Big], \tag{17}$$

where $C = 0.5772\ldots$ is the Euler constant, $z_n = (2\,\alpha\,m_r\,r)/n$ and m_r denotes the reduced mass of the system ($m_r = m_\mu/2$ for the dimuonic atom). The radial integration can be performed by standard formulae. We finally obtain a one-dimensional integral over the v parameter of the Uehling potential. For the $1S$ ground state, we obtain

$$\Delta E_{\rm VPC-T}(1S) = \frac{\alpha}{\pi}\,E_F\,\int_0^1 dv\,\frac{4\,x^2\,(1-v^2/3)}{(2+x\,\sqrt{1-v^2})^3}\,\times$$
$$\times\left[2+\frac{2}{7\,x}\,\frac{1}{\sqrt{1-v^2}}+\frac{3}{7}\,\sqrt{1-v^2}+\left(\frac{4}{7}+\frac{2}{7}\,x\,\sqrt{1-v^2}\right)\,\ln\left(1+\frac{2}{x\,\sqrt{1-v^2}}\right)\right]$$
$$= \frac{\alpha}{\pi}\,(0.605)\,E_F, \tag{18}$$

where

$$x = \alpha\frac{m_\mu}{m_e} = 1.50886\,. \tag{19}$$

For $2S$, a analogous evaluation yields

$$\Delta E_{\rm VPC-T}(2S) = \frac{\alpha}{\pi}\,(0.523)\cdot\frac{E_F}{8}\,. \tag{20}$$

The analytical calculations were partially performed with the computer algebra system MATHEMATICA [22]. The contribution due to the VPC-A diagram can be evaluated by considering the relative contribution of these diagrams to first order hfs (4/7 and 3/7, respectively). An independent evaluation is done by utilization of a spectral decomposition of the reduced Coulomb Green function. If that representation of the Green function is chosen, then the calculation is closely related to [23]. In order to simplify the calculation, we observe that the perturbation can be expressed as a modification of the wave function at $r = 0$. The discrete and continuous spectra give distinct contributions. The results of the respective terms (discrete and continuous spectrum) for the $1S$ and $2S$ states are

$$\Delta E_{\rm VPC-T}(1S) = \frac{\alpha}{\pi}\,E_F\cdot 2\cdot\frac{4}{7}\,\left[\frac{\Delta\psi_{1S}(0)}{\psi_{1S}(0)}\right]_{\mu^+\mu^-} = \frac{\alpha}{\pi}\,[0.04+0.56]\cdot E_F\,, \tag{21}$$

and

$$\Delta E_{\rm VPC-T}(2S) = \frac{\alpha}{\pi}\,\frac{E_F}{8}\cdot 2\cdot\frac{4}{7}\,\left[\frac{\Delta\psi_{2S}(0)}{\psi_{2S}(0)}\right]_{\mu^+\mu^-} = \frac{\alpha}{\pi}\,[-0.14+0.66]\cdot\frac{E_F}{8}\,. \tag{22}$$

The continuous spectrum contribution (second numerical term in Eq. (21) and (22) is very large. It can be understood in the following way. If one would try to omit the energy of the intermediate state in the denominator of the expression

$$\Delta\psi(\mathbf{0}) = \int d^3r\,\overline{G}(E_\psi,\mathbf{0},\boldsymbol{r})V_U(r)\,\psi(\boldsymbol{r})$$
$$= \int d^3r\,\sum_{nl\neq\psi}\frac{\psi_{nl}(\mathbf{0})\,\psi^*_{nl}(\boldsymbol{r})}{E_\psi-E_n}\,V_U(\boldsymbol{r})\,\psi(\boldsymbol{r})$$

in the sense of $E_\psi - E_n \to E_\psi$, then the result should include a divergence in the sum over states. In view of the equation $\sum_{nl\neq\psi}\psi_{nl}(\mathbf{0})\,\psi^*_{nl}(\boldsymbol{r}) = \delta(\boldsymbol{r}) - \psi(\mathbf{0})\,\psi^*(\boldsymbol{r})$ (completeness of the spectum), this is seen as follows:

$$\int d^3r\,\sum_{nl}\frac{1}{E_\psi}\,\psi_{nl}(\mathbf{0})\,\psi^*_{nl}(\boldsymbol{r})\,V_U(\boldsymbol{r})\,\psi(\boldsymbol{r})$$
$$= \frac{V_U(\mathbf{0})-\langle\psi|\,V_U\,|\psi\rangle}{E_\psi}\,\psi(\mathbf{0}),$$

and $V_U(\mathbf{0})$ is a diverging quantitiy. Its apperance means that virtual intermediate states with large wave numbers $k > \alpha\,m_\mu$ are important for the convergence of the integral for $\Delta\psi(\mathbf{0})$, and they lead to a numerically large contribution. The final results for the VPC-T and VPC-A contributions are listed in Table II.

The correction due to the vacuum polarization insertion into the transverse photon line (VPT) is proportional to the matrix element

$$\mathcal{M} = \langle\psi|\boldsymbol{\nabla}^2 V_U|\psi\rangle$$
$$= \frac{\alpha}{\pi}\,\int_0^1 dv\,\frac{v^2\,(1-v^2/3)}{1-v^2}\,\int d^3r\,\Big|\psi(\boldsymbol{r})\Big|^2\,\boldsymbol{\nabla}^2\left[\left(\frac{-\alpha}{r}\right)\exp\left(-\frac{2\,m_e\,r}{\sqrt{1-v^2}}\right)\right]$$
$$= \frac{\alpha}{\pi}\,\int_0^1 dv\,\frac{v^2\,(1-v^2/3)}{1-v^2}\,\int\frac{d^3p}{(2\pi)^3}\,\int\frac{d^3k}{(2\pi)^3}\,\psi^*(\boldsymbol{p})\,\frac{-4\,\pi\,\alpha\,(\boldsymbol{p}-\boldsymbol{k})^2}{(\boldsymbol{p}-\boldsymbol{k})^2+4\,m_e^2/(1-v^2)}\,\psi(\boldsymbol{k}). \tag{23}$$

The matrix element $\mathcal{M}$ is evaluated both in momentum space and in coordinate space with the same result. We obtain for the $1S$ state

$$\mathcal{M}(1S) = \frac{\alpha^2 \left(\alpha\, m_\mu\right)^4}{2\pi} \int_0^1 dv\, \frac{v^2\,(1-v^2/3)}{1-v^2}\, \frac{2\lambda + \alpha\, m_\mu}{(\lambda + \alpha\, m_\mu)^2}\,, \tag{24}$$

where λ is defined in Eq. (6). The final results for VPT (after numerical v-integration) are

$$\Delta E_{\rm VPT}(1S) = \frac{\alpha}{\pi}\, 0.345 \cdot E_F \quad \text{and} \quad \Delta E_{\rm VPT}(2S) = \frac{\alpha}{\pi}\, 0.355 \cdot E_F\,. \tag{25}$$

The results are included in Table II.

The term due to the muonic vacuum polarization in the photon line in the annihilation diagram (denoted "VP-μ-A") is known, since it has the same relative magnitude as that of electronic vacuum polarization in the positronium system. The electronic part (denoted as VP-e-A) is found from the well known asymptotic behavior of the vacuum polarization [11,12]

$$\Delta E_{\rm VPeA}(nS) = \frac{\alpha}{\pi}\, \frac{3}{7}\, \left[\frac{1}{3} \ln \frac{q^2}{m_e^2} - \frac{5}{9} - \frac{\pi}{3}\, i\right] \cdot \frac{E_F}{n^3} \tag{26}$$

for $q^2 = (2\, m_\mu)^2$. The contribution due to the electronic vacuum polarization in the annihilation is the second largest correction to the dimuonium hyperfine splitting in α/π relative units (see Table II, result for VP-e-A). The time-like vector $q = (2\, m_\mu, \mathbf{0})$ is lying in the far time-like asymptotic region for the electronic vacuum polarization. The logarithmic term which appeared originally by the replacement $\ln\left(\boldsymbol{q}^2/m^2\right) \to \ln\left(-q^2/m^2\right)$ (going from space–like to time–like virtual photons) leads to the imaginary part. It can be ascribed to the decay of the ortho state into free electrons ($\mu^+\mu^- \to \gamma \to e^+e^-$)

$$\frac{1}{\Gamma^{(0)}(n^3S_1)} = \tau^{(0)}(n^3S_1) = \frac{6\, n^3}{\alpha^5\, m_\mu} = n^3 \cdot 1.806 \cdot 10^{-12}\,\mathrm{s}\,. \tag{27}$$

In contrast to positronium, the parastate and orthostate lifetime have the same order of magnitude in dimuonium ($\alpha^5\, m_\mu$).

The hadronic contribution (denoted by VP-h-A) to the vacuum polarization is found as the sum of four terms. The main contribution results from a pionic loop. We follow here the approach in [25]. The spectral function is of the form

$$\rho(s) = \frac{(s - 4\, m_\pi^2)^{3/2}}{12\, s^{5/2}}\, |F_\pi(s)|^2\,, \tag{28}$$

where the pionic form factor is used in the form given by Gounaris and Sakurai [26]

$$F_\pi(s) = \frac{N}{D_1 + D_2 - i\, D_3}\,. \tag{29}$$

The quantities N, D_1, D_2 and D_3 are given by

$$N = m_\rho^2 + d m_\rho\, \Gamma_\rho\,, \tag{30}$$

$$d = \frac{3}{\pi}\, \frac{m_\pi^2}{k_\rho^2} \ln \frac{m_\rho + 2\, k_\rho}{2\, m_\pi} + \frac{m_\rho}{2\,\pi\, k_\rho} - \frac{m_\pi^2\, m_\rho}{\pi\, k_\rho^3} \approx 0.48, \tag{31}$$

$$D_1 = m_\rho^2 - s, \quad D_3 = m_\rho\, \Gamma_\rho \left(k(s)/k_\rho\right)^3\, m_\rho/\sqrt{s}, \tag{32}$$

$$D_2 = \Gamma_\rho \frac{m_\rho^2}{k_\rho^3} \left[k(s)^2\, \left(h(s) - h_\rho\right) + k_\rho^2\, h'(m_\rho^2)\, \left(m_\rho^2 - s\right)\right], \tag{33}$$

where h' denotes the derivative of h, and the functions k and h are defined as

$$k(s) = \frac{1}{2}\sqrt{s - 4m_\pi^2}, \quad h(s) = \frac{2}{\pi}\,\frac{k(s)}{\sqrt{s}}\,\ln\left(\frac{\sqrt{s} + 2\,k(s)}{2\,m_\pi}\right). \tag{34}$$

with the special values $k_\rho \equiv k(m_\rho^2)$, $h_\rho \equiv h(m_\rho^2), \Gamma_\rho = 150.7(1.2)\,\mathrm{MeV}, m_\rho = 768.5(6)\,\mathrm{MeV}$ [15]. We give results for the $1S$ state only in the sequel. The $1/n^3$ scaling is easily restored in the final result. The contribution from the pionic vacuum polarization is given by

$$\Delta E_{\pi^+\pi^-}(1S) = \frac{\alpha}{\pi}\,\frac{3}{7}\left[4\,m_\mu^2\int_{4\,m_\pi^2}^{\infty} ds\,\frac{\rho(s)}{4\,m_\mu^2 - s}\right] E_F = \frac{\alpha}{\pi}\,(-0.055)\cdot E_F\,. \tag{35}$$

In the simple ρ-meson pole approximation, where $\rho(s) = 4\pi^2/f_\rho^2\,\delta(s - m_\rho^2)$ with $f_\rho^2/(4\,\pi) = 2.2$ [27], we have

$$\Delta E_{\pi^+\pi^-}(1S) \approx \Delta E_\rho(1S) = \frac{\alpha}{\pi}\,(-0.050)\,E_F\,. \tag{36}$$

This result agrees with the full pion form factor of (29) to about 10 %, so it is justified to consider mesonic resonances of higher energy in the pole approximation only. The higher energy mesonic contributions are due to the ω and ϕ resonances. These resonances are not included in the Gounaris-Sakurai form factor and are treated separately. Estimating the coupling constants as $f_\omega^2/(4\pi) = 18(2)$, $f_\phi^2/(4\pi) = 11(2)$ [25,27] and given the meson masses of $m_\omega = 782\,\mathrm{MeV}$, $m_\phi = 1019\,\mathrm{MeV}$ [15], the results are

$$\Delta E_\omega(1S) = \frac{\alpha}{\pi}\,(-0.006)\cdot E_F \quad \text{and} \quad \Delta E_\phi(1S) = \frac{\alpha}{\pi}\,(-0.005)\cdot E_F\,. \tag{37}$$

The background above 1 GeV is estimated by assuming a form of

$$\rho(s) = \frac{R}{3\,s}, \quad \text{where} \quad R = \frac{\sigma(e^+\,e^- \to \text{hadrons})}{\sigma(e^+\,e^- \to \mu^+\,\mu^-)}\,, \tag{38}$$

for the spectral function with a branching ratio $R \approx 2$ (constant) below $\sqrt{s} = 4\,\mathrm{GeV}$ and $R \approx 4$ above $\sqrt{s} = 4\,\mathrm{GeV}$ (see [15], p. 190). Integrating from an estimated lower threshold of $s_{\rm th} \approx (1\,\mathrm{GeV})^2$ we obtain

$$\Delta E_>(1S) \approx \frac{\alpha}{\pi}\,(-0.014)\cdot E_F. \tag{39}$$

Summing all contributions and restoring the $1/n^3$ scaling, we have as the contribution from the hadronic vacuum polarization

$$\Delta E_{\rm VP-h-A}(nS) = \Delta E_\pi + \Delta E_\omega + \Delta E_\phi + \Delta E_> = \frac{\alpha}{\pi}\,[-0.080(9)]\,\cdot\,\frac{E_F}{n^3}\,. \tag{40}$$

We estimate model-dependent uncertainties in the hadronic vacuum polarization to be of the order of 11 %. The hadronic term is included in Table II (result for VP-h-A).

The sum of all corrections (see Table II) to the hyperfine splitting in dimuonium amounts to

$$\Delta E_{\rm hfs}(1S) = \frac{\alpha}{\pi}\,0.689(9)\cdot E_F \quad \text{and} \quad \Delta E_{\rm hfs}(2S) = \frac{\alpha}{\pi}\,0.556(9)\cdot\frac{E_F}{8}\,. \tag{41}$$

In the final results for hyperfine splitting, we estimate higher order corrections to enter at the 5% level of the next–to–leading order contributions. We obtain

$$E_{\rm hfs}(1S) = 4.23283(35)\cdot 10^7\,\mathrm{MHz} \tag{42}$$

and

$$E_{\rm hfs}(2S) = 5.28941(34)\cdot 10^6\,\mathrm{MHz}\,. \tag{43}$$

Results for the Lamb shift and the hyperfine structure of low-lying levels are presented in Tables I and II. The largest deviation from the scaling appeared in VPC-T and VPC-A contributions (16%), because the wave function (see Eqs. (21) and (22)) is more sensitive to the behaviour of the potential about the origin.

An important point for a possible investigation of the spectrum is the lifetime of levels. As one can see from Eqs. (13) and (27) the annihilation lifetimes of S-levels are much shorter that the lifetime of the free muon, $\tau_\mu = 2.20\,10^{-6}\,s$.

By contrast, the annihilation decay rate for P-states includes an extra α^2, and the lifetime is of the same order of magnitude as that of the free muon.

The decay rates of excited states have to be compared with the atomic transition rates, which are also of the order of $\alpha^5\, m_\mu$ (see e. g. [16]). We obtain

$$\tau(2P \to 1S) = 1.54 \cdot 10^{-11}\,\mathrm{s}\,. \tag{44}$$

Annihilation of P states is suppressed by two orders of α compared to S states due to the behaviour of the P wave function near the origin. Therefore, the annihilation lifetime of the $2P$ state can be estimated to be of the order of $10^{-7}\,\mathrm{s}$, and it is seen that the atomic transition, not the annihilation, determines the lifetime of the excited $2P$ state in dimuonium.

This situation is different for S states, where the annihilation dominates over atomic transitions. The annihilation lifetimes of of $1S$ and $2S$ states lie between $0.6 \cdot 10^{-12}\,\mathrm{s}$ and $14 \cdot 10^{-12}\,\mathrm{s}$, and we expect that the decay rates could be measured via detection of the decay products. Radiative corrections to the decay rates are considered in the following Section.

IV. DECAY CHANNELS OF ORTHODIMUONIUM

The leading–order contributions to the orthodimuonium and paradimuonium decay rate can be extracted as the imaginary parts of the energy corrections to the hyperfine structure,

$$\Gamma^{(0)}(n^3S_1) = \frac{\alpha^5\, m_\mu}{6\, n^3} \quad \text{and} \quad \Gamma^{(0)}(n^1S_0) = \frac{\alpha^5\, m_\mu}{2\, n^3}\,. \tag{45}$$

The calculations at leading order were presented above (Eqs. (13, 27)). The above results can also be found in [3,4].

We begin the consideration of radiative corrections with orthodimuonium, and provide results for the $1S$ state here. Results for the $2S$ state (and $1S$) are summarized in Table III. The diagrams contributing in next–to–leading order for ortho states are depicted in Fig. 7.

The VPC-A correction can be interpreted as a modification of the wave function at the origin. The energy shift and decay rate are both proportional to $|\psi(\mathbf{0})|^2$. The annihilation diagram contributes $3/7\, E_F$ to the first–order result for the hyperfine splitting. Hence, the VPC-A diagram yields a correction of

$$\Delta\Gamma_{\mathrm{VPC-A}}(1^3S_1) = \frac{\alpha}{\pi}\left[\frac{7}{3}\cdot 0.454\right]\,\Gamma^{(0)}(1^3S_1) = \frac{\alpha}{\pi} 1.06 \cdot \Gamma^{(0)}(1^3S_1) \tag{46}$$

to the decay rate. Analogous considerations are true for the Vert-A correction, because the diagrams consist of separated blocks, and hence the correction to hfs and to the decay rate can be traced back to the same matrix element of the wave function. We obtain

$$\Delta\Gamma_{\mathrm{Vert-A}}(n^3S_1) = -4\,\frac{\alpha}{\pi}\cdot\Gamma^{(0)}(n^3S_1)\,. \tag{47}$$

The diagrams VP-μ-A, VP-e-A and VP-h-A have to be interpreted as modifications of the photon propagator. Because the energy shift is proportional to the amplitude of the propagator, but the decay rate is proportional to its square, we have to multiply the relative correction to hfs by a factor of 2 in order to obtain the relative correction to the decay rate. Hence, the VP-μ-A, VP-e-A and VP-h-A diagrams yield a total correction of

$$\frac{\alpha}{\pi}\left[-\frac{16}{9} + \frac{4}{3}\ln\left(2\frac{m_\mu}{m_e}\right) - \frac{10}{9} - 0.37(4)\right]\cdot\Gamma^{(0)}(n^3S_1)$$

to the decay rate.

We now consider the one-loop radiative corrections to the electron line (ReA) and emission of a photon by an electron, i. e. bremsstrahlung (BeA). The sum of BeA+ReA can be easily obtained from the diagrams in Fig. 8 for the two-loop electron polarization correction to the hyperfine splitting, which is completely determined by the asymptotic behaviour of the two-loop vacuum polarization (see e. g. [13]). For the correction to the hyperfine splitting, we obtain

$$\Delta E_{\mathrm{VP-2}}(nS) = \frac{\alpha^2}{\pi^2}\,\frac{3}{7}\,\left[\frac{1}{4}\ln\frac{q^2}{m_e^2} + \left(\zeta(3) - \frac{5}{24}\right) - \frac{\pi}{4}\,i\right]\frac{1}{n^3}\cdot E_F\,, \tag{48}$$

where $q^2 = 4m_\mu^2$ and $\zeta(3) = 1.202\ldots$ is the Riemann ζ function of argument 3. This correction is of relative order α^2/π^2 with respect to E_F and was therefore not considered in Section III. The imaginary part of this contribution is just the result for the sum of the diagrams ReA+BeA. The correction to the decay rate can now be evaluated easily. The sum of ReA+BeA yields a correction of

$$\frac{3}{4}\,\frac{\alpha}{\pi}\cdot\Gamma^{(0)}(n^3S_1)$$

relative to the leading order result (cf. Eqs. (26,45)).

The last term in relative order α/π is the three-photon annihilation. The result is known from orthopositronium calculations [28] (see also [16,12]):

$$\Delta\Gamma_{3A}(n^3S_1) = \frac{2\alpha^6}{\pi}\,\frac{1}{n^3}\,\frac{\pi^2-9}{9}\,m_\mu = \frac{\alpha}{\pi}\,\left[\frac{4}{3}\left(\pi^2-9\right)\right]\cdot\Gamma^{(0)}(n^3S_1)\,. \tag{49}$$

The final result for the $1S$ decay (see also Table III) is

$$\begin{aligned}
\Delta\Gamma(1^3S_1) &= \frac{\alpha}{\pi}\,\left[\left(\frac{4}{3}\ln\frac{2\,m_\mu}{m_e} - \frac{221}{36}\right) + \Big(0.68(4)\Big) + \left(\frac{4\,(\pi^2-9)}{3}\right)\right]\,\Gamma^{(0)}(1^3S_1) \\
&\approx \frac{\alpha}{\pi}\left\{\Big(1.90\Big) + \Big(0.68(4)\Big) + \Big(1.16\Big)\right\}\Gamma^{(0)}(1^3S_1) \\
&= \frac{\alpha}{\pi}\,3.74(4)\cdot\Gamma^{(0)}(1^3S_1)\,.
\end{aligned} \tag{50}$$

The first term corresponds to the sum of the analytically evaluated contributions Vert-A, VP-μ-A, VP-e-A and BeA+ReA, and has the numerical value 1.90. The second term originates from the numerically evaluated contributions VPC-A and VP-h-A. The last term is associated to the three photon decay. The result in Eq. (50) has to be compared with the earlier analysis of the decay rate of heavy leptonium [4]. The final result for the analytically evaluated contributions, which is identical to the first term in Eq. (50), whose analytical expression is $(4/3)\,\ln(2\,m_\mu/m_e) - 221/36$, is found in agreement with the pioneering investigations by J. Malenfant [4]. For the VPC-A correction, Malenfants results are in slight numerical disagreement with ours (see Eqs. (77,78) in [4]). We presume this disagreement can be traced to the fact that Malenfant has calculated the VPC-A correction with free Green functions, whereas the evaluation in this work is done using bound Green functions. In this context it is important to note that in the limit of $\alpha\,m_\mu/2m_e \to 0$, our result is agreement with that of Malenfant. This can be seen as follows. The VPC-A correction may be rewritten as a correction $\Delta\psi(0)$ to the wave function at the origin. After this reinterpretation, we find

$$\Delta\psi(0) = \frac{\alpha}{\pi}\,\left(\frac{3\,\pi}{16}\,\kappa + O(\kappa^2)\right)\,\psi(0) \quad \text{for} \quad \kappa = \frac{\alpha\,m_\mu}{2\,m_e} \to 0\,, \tag{51}$$

which is in agreement with Eq. (80) of [4]. We can therefore conclude that in the limit of weak binding ($\kappa \to 0$), Malenfants result is in agreement with ours. However, we hold the view that bound Green functions should rather be used for the VPC-A correction. The atomic momentum in dimuonium is of the order of $\alpha\,m_\mu/2 = \kappa\,m_e$ ($\kappa \approx 0.75$). This momentum is close to the mass of the loop particles (electrons and positrons) of electronic vacuum polarization. These particles determine the radius of the Uehling potential. Therefore, some of the momentum integration for the VPC-A correction is performed in an area about m_e, where the bound Coulomb Green function cannot be approximated by the free Green function (because the effect of the binding Coulomb potential, in momentum space, is inversely proportional to the square of the momentum transfer). This consideration should explain the slight numerical disagreement for the VPC-A correction between this work and the result in [4].

The sum of next–to–leading order corrections to the decay rate for the $2S$ state is (see Table III)

$$\Delta\Gamma(2^3S_1) = \frac{\alpha}{\pi}\,3.60(4)\cdot\Gamma^{(0)}(2^3S_1)\,. \tag{52}$$

We estimate the higher order corrections to be suppressed by an additional factor of α compared to the next–to–leading order result. We obtain the following results for the decay rate of orthodimuonium, taking into account also the uncertainty from our model of the hadronic vacuum polarization:

$$\tau(1^3S_1) = 1.79073(77)\cdot10^{-12}\,\text{s} \quad \text{and} \quad \tau(2^3S_1) = 14.3305(59)\cdot10^{-12}\,\text{s}. \tag{53}$$

V. DECAY CHANNELS OF PARADIMUONIUM

The diagrams contributing to paradimuonium decay in next–to–leading order $\alpha^6\, m$ are presented in Fig 9, results are summarized in Table IV. The vertex correction term (Vert-2A) is equivalent to the corresponding correction for parapositronium [30],

$$\Delta\Gamma_{\rm Vert-2A}(n^1S_0) = -\frac{\alpha}{\pi}\,\frac{20-\pi^2}{4}\,\Gamma^{(0)}(n^1S_0)\,. \tag{54}$$

The correction to the wave function caused by the VPC-A diagram modifies the decay rate of the para system in the same way as the ortho system (see Table IV), and introduces a deviation from the $1/n^3$ scaling.

For the para state, there exists another correction to the decay rate corresponding to the decay into a photon and an electron-positron pair. The result for the A2e correction can be obtained in the following way. We consider the one–loop vacuum polarization insertion into a 2-photon annihilation diagram (Fig. 10). Because the vacuum polarization insertion, evaluated for a real photon, must be equal to zero (gauge invariance of vacuum polarization), the imaginary part of the diagrams in Fig. 10 leads to the result we need. We can use Eq. (4) for the parametric form of the vacuum polarization insertion, and we consider the s-integration as the final one. The integrand is now equivalent to the imaginary part of the 2A diagram for the hfs, but with one of the photons having a finite mass s (s corresponds to the sum of the four–momenta of the emerging electron–positron pair). The vacuum polarization insertion normally fixes a gauge (the Landau gauge) for the virtual photon, because the polarization insertion is proportional to the transverse projector. However, as it was demonstrated in [31], it is possible to substitute in Eq. (4) any covariant gauge. For convenience, we choose the Feynman gauge. As a result we have the expression

$$\Delta\Gamma_{\rm A2e}(n^1S_0) = \frac{\alpha}{\pi}\int ds\,\rho(s)\,\Gamma^{(0)}(s,0)\,, \tag{55}$$

where $\Gamma^{(0)}(s,0)$ is the decay rate to one real photon and a virtual photon with mass s. In order to obtain the correction in relative units, we divide by the first–order result, which is given by $\Gamma^{(0)}(0,0)$. The correction relative to the first–order result $\Gamma^{(0)}(n^1S_0)$ is given by

$$\frac{\Delta\Gamma_{\rm A2e}(n^1S_0)}{\Gamma^{(0)}(n^1S_0)} = 2\,\frac{\alpha}{\pi}\int ds\,\rho(s)\,\frac{\Gamma^{(0)}(s,0)}{\Gamma^{(0)}(0,0)}\,, \tag{56}$$

An additional factor 2 appears because the insertion of a vacuum polarization operator doubles the number of non-equivalent diagrams contributing to the imaginary part. For the logarithmic coefficient we may neglect s in $\Gamma^{(0)}(s,0)$ and approximate $\Gamma^{(0)}(s,0) \to \Gamma^{(0)}(0,0)$, and use the asymptotic form of the spectral function (cf. Eq (2)),

$$\rho(s) \to \frac{1}{3\,s} \quad \text{for} \quad s \to \infty\,.$$

We can thus easily obtain the logarithmic coefficient,

$$\frac{\Delta\Gamma_{\rm A2e}(n^1S_0)}{\Gamma^{(0)}(n^1S_0)} \approx 2\int_{(2\,m_e)^2}^{\Lambda^2=(2\,m_\mu)^2} ds\,\frac{1}{3\,s} = 2\,\frac{1}{3}\,\ln\frac{m_\mu^2}{m_e^2} = \frac{4}{3}\,\ln\frac{m_\mu}{m_e}\,.$$

The full result requires a more detailed analysis of the dependence of $\Gamma^{(0)}(s,0)$ on s. It differs from the approximate analysis presented above only by an additive constant. The final result of the calculation is

$$\Delta\Gamma_{\rm A2e}(n^1S_0) = \frac{\alpha}{\pi}\,\left(\frac{4}{3}\ln\frac{2m_\mu}{m_e} - \frac{16}{9}\right)\,\frac{1}{n^3}\cdot\Gamma^{(0)}(n^1S_0)\,. \tag{57}$$

An independent evaluation of the A2e-correction using the standard S-matrix formalism is used to verify the result in Eq. (57). Treatment of the Dirac currents involved in simplified by application of a symbolic program [32] developed for high energy physics calculations by A. Hsieh and E. Yehudai. Some care must be taken during evaluation, because one cannot assume the electrons as massless in the final states (the result else includes a logarithmic divergence in the electron mass). Proper regularization of the relevant expression then leads to the result in Eq. (57).

The final result for the next–to–leading order radiative corrections to paradimuonium decay (see Table IV) is

$$\Delta\Gamma(1^1S_0) = \frac{\alpha}{\pi}\,4.79\cdot\Gamma^{(0)}(1^1S_0)\,. \tag{58}$$

For the $2S$ state, we have

$$\Delta\Gamma(2^1S_0) = \frac{\alpha}{\pi}\, 4.65 \cdot \Gamma^{(0)}(2^1S_0)\,. \tag{59}$$

Estimating higher order corrections to enter at the level of 5% of the next–to–leading order contributions, we obtain the following theoretical values for the paradimuonium decay:

$$\tau(1^1S_0) = 0.59547(33) \cdot 10^{-12}\,\mathrm{s} \quad \text{and} \quad \tau(2^1S_0) = 4.7653(25) \cdot 10^{-12}\,\mathrm{s}\,. \tag{60}$$

VI. CONCLUSIONS

We evaluate next–to–leading order corrections to the spectrum, to the hyperfine splitting and to the decay rate of low-lying levels of the dimuonic system. The results for the spectrum are given in Section II. We observe that for $2P$ states, the atomic decay into the $1S$ state dominates over annihilation processes. This would facilitate experimental observation of the atomic transition, if dimuonium atoms can be produced in quantities sufficient to carry out spectroscopic measurements. We evaluate the hyperfine splitting of $1S$ and $2S$ states in next–to–leading order. The results are

$$E_{\rm hfs}(1S) = \left[1 + \frac{\alpha}{\pi}\, 0.689(9)\right]\, \frac{7}{12}\, \alpha^4\, m_\mu = 4.23283(35) \cdot 10^7\,\mathrm{MHz} \tag{61}$$

and

$$E_{\rm hfs}(2S) = \left[1 + \frac{\alpha}{\pi}\, 0.556(9)\right]\, \frac{7}{12}\, \alpha^4\, m_\mu = 5.28941(34) \cdot 10^6\,\mathrm{MHz}\,. \tag{62}$$

We present a complete evaluation of all next–to–leading order radiative corrections to the lifetime of both the ortho– and para–state of the dimuonic atom. In leading order, we reproduce the known results [3,4]

$$\Gamma(n^3S_1) = \frac{\alpha^5\, m_\mu}{6\, n^3} \quad \text{and} \quad \Gamma(n^1S_0) = \frac{\alpha^5\, m_\mu}{2\, n^3} \tag{63}$$

as imaginary contributions to the hyperfine splitting (Eqs. (13, 27)).

The results in next–to–leading order are for orthodimuonium,

$$\Gamma(1^3S_1) = \left[1 + \frac{\alpha}{\pi}\, 3.74(4)\right] \Gamma^{(0)}(1^3S_1) \quad \text{and} \quad \Gamma(2^3S_1) = \left[1 + \frac{\alpha}{\pi}\, 3.60(4)\right] \Gamma^{(0)}(2^3S_1)\,, \tag{64}$$

where the primary theoretical uncertainty is due to hadronic vacuum polarization. The lifetimes of orthostates are given by

$$\tau(1^3S_1) = 1.79073(77) \cdot 10^{-12}\,\mathrm{s} \quad \text{and} \quad \tau(2^3S_1) = 14.3305(59) \cdot 10^{-12}\,\mathrm{s}\,. \tag{65}$$

For paradimuonium, we obtain

$$\Gamma(1^1S_0) = \left[1 + \frac{\alpha}{\pi}\, 4.79\right] \Gamma^{(0)}(1^1S_0) \quad \text{and} \quad \Gamma(2^1S_0) = \left[1 + \frac{\alpha}{\pi}\, 4.65\right] \Gamma^{(0)}(2^1S_0)\,. \tag{66}$$

The lifetimes are given by

$$\tau(1^1S_0) = 0.59547(33) \cdot 10^{-12}\,\mathrm{s} \quad \text{and} \quad \tau(2^1S_0) = 4.7653(25) \cdot 10^{-12}\,\mathrm{s}\,. \tag{67}$$

We estimate higher order QED corrections to enter at the 5% level of the next–to leading order corrections considered in this work.

Lifetimes in the $10^{-12}\,\mathrm{s}$ range can be measured by established methods of particle physics via detection of the decay products (electron-positron pairs in case of orthodimuonium and two photons in the case of paradimuonium). We stress that accurate decay rate measurements can be accomplished with fewer individual atoms than would be needed for spectroscopic investigations.

One of the ways to investigate the hyperfine structure of $1S$ or $2S$ states could be based on the observation of the interference between paradimuonium and orthodimuonium in an infrared frequency field at resonance (the radiofrequency field would mix the two states and thus yield a modified decay rate of the statistical sample). We conclude that the dimuonic system offers the possibility to observe quantum electrodynamic effects in a previously unexplored kinematic region.

ACKNOWLEDGMENTS

G. S. and U. J. thank DFG for continued support (contract no. SO333/1-2). The work of S. K. and V. I. has been supported in part by the Russian Foundation for Basic Research (grant #95-02-03977). S. K. is grateful for hospitality at the Technical University of Dresden. The authors would like to thank V. V. Vereshagin, V. A. Shelyuto, P. Mohr and J. Malenfant for stimulating discussions. We also acknowledge helpful discussions with M. Sander and S. Vigdor.

[1] L. Nemenov, Yad. Fiz. **15**, 1047 (1972) (in Russian), Sov. J. Nucl. Phys. **15**, 582 (1972).
[2] S. Bilenkii, N. van Hieu, L. Nemenov and F. Tkebuchava, Yad. Fiz. **10**, 812 (1969) (in Russian), Sov. J. Nucl. Phys. **10**, 469 (1969).
[3] J. Malenfant in *AIP Conf. Proc.* **150**, p. 595, AIP, New York (1986).
[4] J. Malenfant, Phys. Rev. D **36**, 863 (1987).
[5] S. Wycech, and A. M. Green, Nucl. Phys. **A562**, 446 (1993); Z. K. Silagadze, ZhETF **60** 673, (1994) (in Russian); JETP Lett. **60**, 689 (1994).
[6] V. Lyubovitskij and A. Rusetsky, Phys. Lett. **B389**, 181 (1996).
[7] O. E. Gorchakov, A. V. Kuptsov, L. L. Nemenov and D. Yu. Riabkov, Yad. Fiz. **59**, 2015 (1996); Phys. At. Nucl. **59**, 1942 (1996).
[8] L. G. Afanasyev, A. S. Chvyrov, O. E. Gorchakov, M. A. Ivanov, V. V. Karpukhin, A. V. Kolomyichenko, V. I. Komarov, V .V. Kruglov, A. V. Kuptsov, L. L. Nemenov, M. V. Nikitin, Zh. P. Pustylnik, A. V. Kulikov, S. V. Trusov, V. V. Yazkov, G. G. Mkrtchya, and A. P. Kurov, Phys. Lett. **B308**, 200 (1993); L. G. Afanasyev, A. S. Chvyrov, O. E. Gorchakov, V. V. Karpukhin, A. V. Kolomyichenko, V. I. Komarov, V .V. Kruglov, A. V. Kuptsov, L. L. Nemenov, M. V. Nikitin, Zh. P. Pustylnik, A. V. Kulikov, S. V. Trusov and V. V. Yazkov, Phys. Lett. **B338**, 478 (1994).
[9] L. G. Afanasyev, A. S. Chvyrov, V. V. Karpukhin, V. I. Komarov, A. V. Kolomyichenko, V .V. Kruglov, A. V. Kuptsov, L. L. Nemenov, M. V. Nikitin, M. N. Shumakov, S. M. Frolikov, Zh. P. Pustylnik, O. E. Gorchakov, A. V. Kulikov, S. V. Trusov, K. I. Gubrienko and V. I. Kotov, Phys. Lett. **B236**, 116 (1990); L. G. Afanasyev, O. E. Gorchakov, V. V. Karpukhin, V. I. Komarov, A. V. Kolomyichenko, V .V. Kruglov, A. V. Kulikov, A. V. Kuptsov, L. L. Nemenov, M. V. Nikitin, Zh. P. Pustylnik, S. V. Trusov, M. N. Shumakov, S. M. Frolikov and A. S. Chvyrov, Yad. Fiz. **51**, 1040 (1990) (in Russian); Sov. J. Nucl. Phys. **51**, 664 (1990).
[10] R. Coombes, R. Flexer, A. Hall, R. Kennelly, J. Kirkby, R. Piccioni, D. Porat, M. Schwartz, R. Spitzer, J. Toraskar, S. Wiesner, B. Budnick and J. W. Kats, Phys. Rev. Lett. **37**, 249 (1976); S. H. Aronson, R. H. Bernstein, G. J. Bock, R. D. Cousins, Jr., J. F. Greenhalghm D. Hedin, M. Schwartz, T. K. Shea, G. B. Thomson and B. Winstein, Phys. Rev. Lett. **48**, 1078 (1982); S. H. Aronson, R. H. Bernstein, G. J. Bock *et al.,* Phys. Rev. **D33**, 3180 (1986).
[11] V. B. Berestetskii, E. M. Lifshitz and L. P. Pitaevskii. *Quantum Electrodynamics*. Pergamon Press, Oxford, 1982.
[12] C. Itzykson ane J.-B. Zuber, *Quantum Field Theory*, McGraw Hill , N. Y., 1980.
[13] J. Schwinger, *Particles, Sources and Fields*, Addison-Wesley, Reading (MA), 1970.
[14] E. R. Cohen and B. N. Taylor, Rev. Mod. Phys. **59**, 1121 (1987).
[15] R. M. Barnett et al., Phys. Rev **D 54**, 1 (1996).
[16] H. A. Bethe and E. E. Salpeter, *Quantum Mechanics of One- and Two-Electron Atoms*. Springer-Verlag, Berlin (1957).
[17] R. A. Ferrell, Phys. Rev. **84**, 858 (1951).
[18] J. Pirenne, Arch. Sci. Phys. Nat. **28**, 273 (1946); **29**, 121, 207, 265 (1947).
[19] V. B. Berestetskii and L. D. Landau, JETP (USSR) **19**, 673 (1949); V. B. Berestetskii, JETP (USSR) **19**, 1130 (1949).
[20] R. Karplus and A. Klein, Phys. Rev. **87**, 848 (1952); T. Fulton and P. C. Martin, Phys. Rev. **95**, 811 (1954).
[21] J. A. Wheeler, Ann. New Acad. Sci. **95**, 219 (1946).
[22] S. Wolfram, "Mathematica-A System for Doing Mathematics by Computer", Addison-Wesley, Reading (MA), 1988.
[23] S. G. Karshenboim and V. G. Ivanov, *to be published in Phys. Lett. A.*
[24] V. G. Ivanov and S. G. Karshenboim, ZhETF **109**, 1219 (1996) (in Russian); JETP **82**, 656 (1996); Phys. Lett. **A210**, 313 (1996).
[25] J. R. Sapirstein, E. A. Terray, D. R. Yennie, Phys. Rev. D **29**, 2290 (1984).
[26] G. J. Gounaris and J. J. Sakurai, Phys. Rev. Lett. **21**, 244 (1968).
[27] T. H. Bauer, R. D. Spital, D. R. Yennie and F. M. Pipkin, Rev. Mod. Phys. **50**, 261 (1978).
[28] A. Ore and J. Powell, Phys. Rev. **75**, 1696 (1949).
[29] R. Van Royen and V. F. Weisskopf, Nuovo Cim. **L**, 615 (1967).
[30] I. Harris and L. M. Brown, Phys. Rev. **105**, 1656 (1957).
[31] S. G. Karshenboim, Yad. Fiz. **56**, 115 (1993) (in Russian); Phys. At. Nucl. **56**, 777 (1993).
[32] A. Hsieh and E. Yehudai, Computers in Physics (peer–reviewed journal section) **6**, 253 (1992).

state	C	$\mathcal{L}$
1S	-0.15	-0.49 eV
2S	-0.018	-0.058 eV
2P	-.000043	-0.0014 eV

TABLE I. Contributions to the Lamb shift due to the electronic vacuum polarization. C is given in relative units, $\Delta E = \frac{\alpha}{\pi} C E_0$, where E_0 is the Rydberg constant for the dimuonic atom.

diagram	$C(1S)$	$8\,C(2S)$
(g-2)-T	0.571	0.571
Rec	-0.857	-0.857
Vert-A	-1.714	-1.714
VP-μ-A	-0.381	-0.381
2A	0.263	0.263
VPC-T	0.605	0.523
VPT	0.345	0.355
VPC-A	0.454	0.393
VP-e-A	1.483	1.483
VP-h-A	-0.080(9)	-0.080(9)
Sum	0.689(9)	0.556(9)

TABLE II. Corrections of relative order α/π to the dimuonium hyperfine splitting. All contributions are explained in the text. The corrections (g-2)-T, Rec, Vert-A, VP-μ-A and 2A contribute to the positronium hyperfine splitting just as in dimuonium. The remaining contributions (VPC-T, VPT, VPC-A, VP-e-A, VP-h-A) are specific to the dimuonic system. Results are given in relative units $\Delta E = \alpha/\pi\, C\, E_F$.

diagram	$C(1S)$	$8\,C(2S)$
Vert-A	-4.00	-4.00
VPC-A	1.06	0.92
VP-μ-A	-1.78	-1.78
VP-e-A	6.92	6.92
VP-h-A	-0.37(4)	-0.37(4)
BeA+ReA	0.75	0.75
3A	1.16	1.16
Sum	3.74(4)	3.60(4)

TABLE III. Corrections of relative order α/π to the orthodimuonium decay. Results are given in relative units $\Delta\Gamma(n^3S_1) = \alpha/\pi\, C\, \Gamma^{(0)}(1^3S_1)$.

diagram	$C(1S)$	$8\,C(2S)$
Vert-2A	-2.53	-2.53
VPC-2A	1.06	0.92
A2e	6.26	6.26
Sum	4.79	4.65

TABLE IV. Corrections of relative order α/π to the paradimuonium decay. Results are given in relative units $\Delta\Gamma(n^1S_0) = \alpha/\pi\, C\, \Gamma^{(0)}(1^1S_0)$.

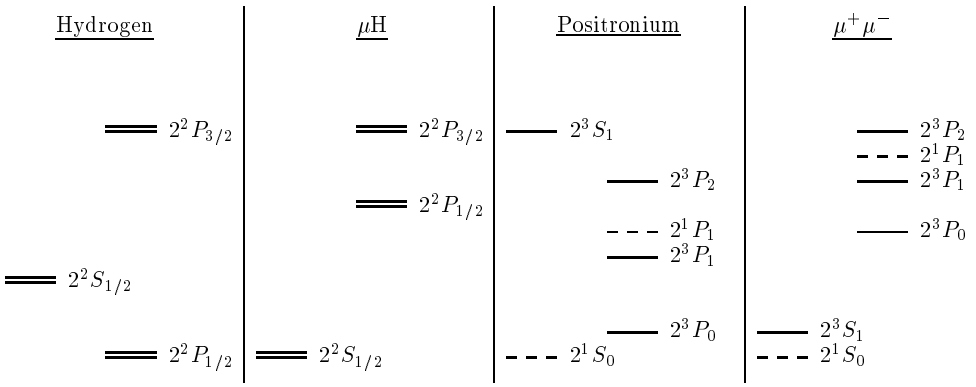

FIG. 1. Overview over the spectrum of $n = 2$ levels in hydrogen, muonic hydrogen (μH), positronium and dimuonium ($\mu^+\mu^-$). The double lines denote the hyperfine structure splitting of the levels in hydrogen and muonic hydrogen. Dashed lines denote $S = 0$-states, full lines denote $S = 1$-states.

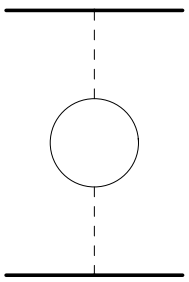

FIG. 2. (Electronic) vacuum polarization insertion in the Coulomb photon (main contribution to the Lamb shift in muonic systems). The dashed line denotes a Coulomb photon. Bold fermionic lines denote muons, thin lines denote electrons and positrons.

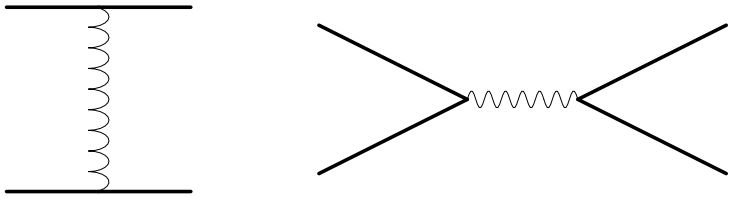

FIG. 3. Transverse photon exchange diagram and (time-like) photon annihilation diagram. Both of the diagrams contribute to the hyperfine structure of S states in leading order. The zig-zag line denotes a transverse photon, the wavy line denotes the full photon propagator.

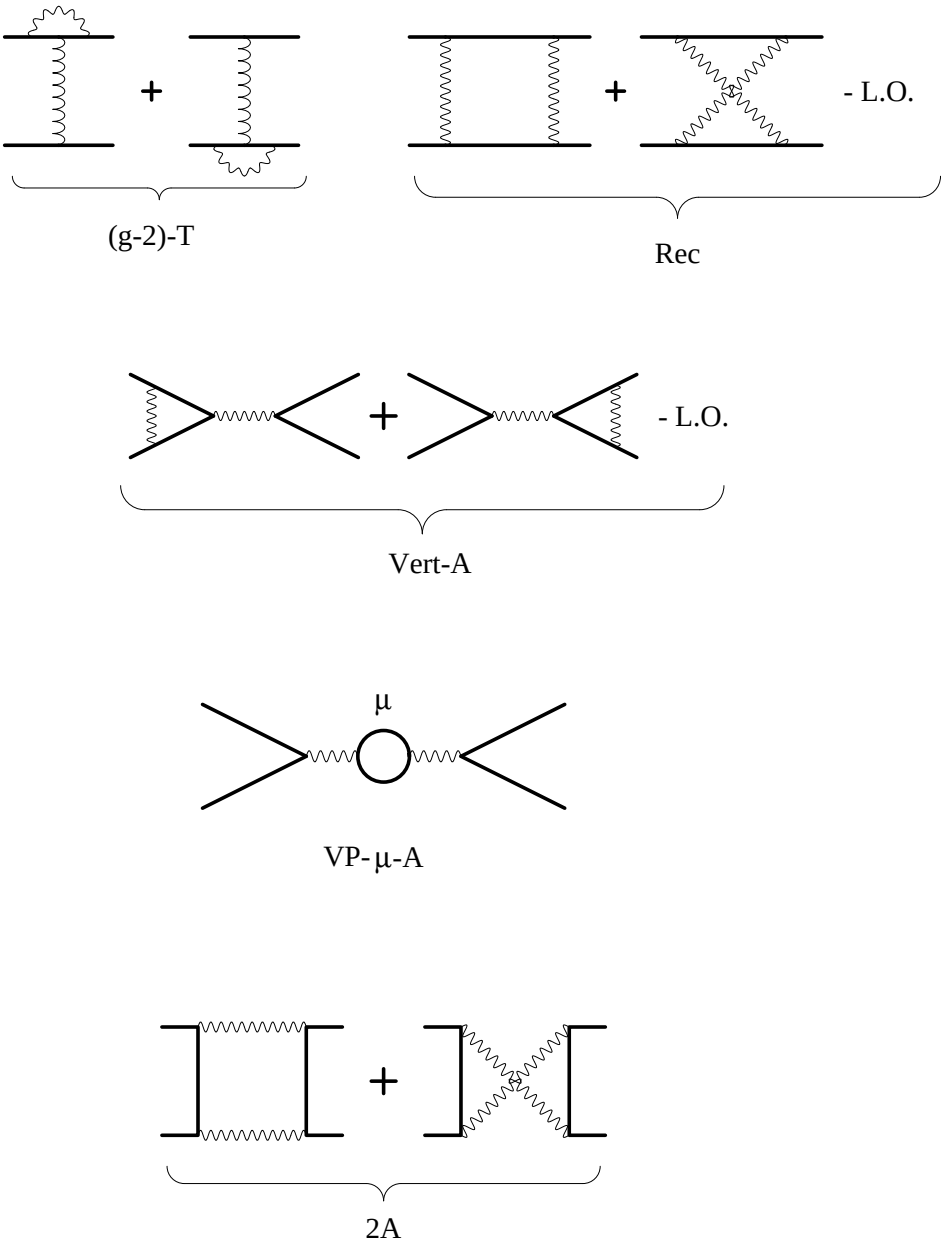

FIG. 4. Known corrections up to the order $\alpha/\pi\, E_F$ to the hyperfine splitting of dileptonic systems (positronium, dimuonium). Diagrams are explained in the text. For the dimuonic atom, the corrections depicted here contribute to hfs, but there are additional terms specific to the dimuonic system which need to be taken into account. The subtraction of lower order (L.O.) contributions is necessary for some of the diagrams in order to prevent double counting. The bold fermionic lines denote muons. The direction of time in all diagrams is from left to right.

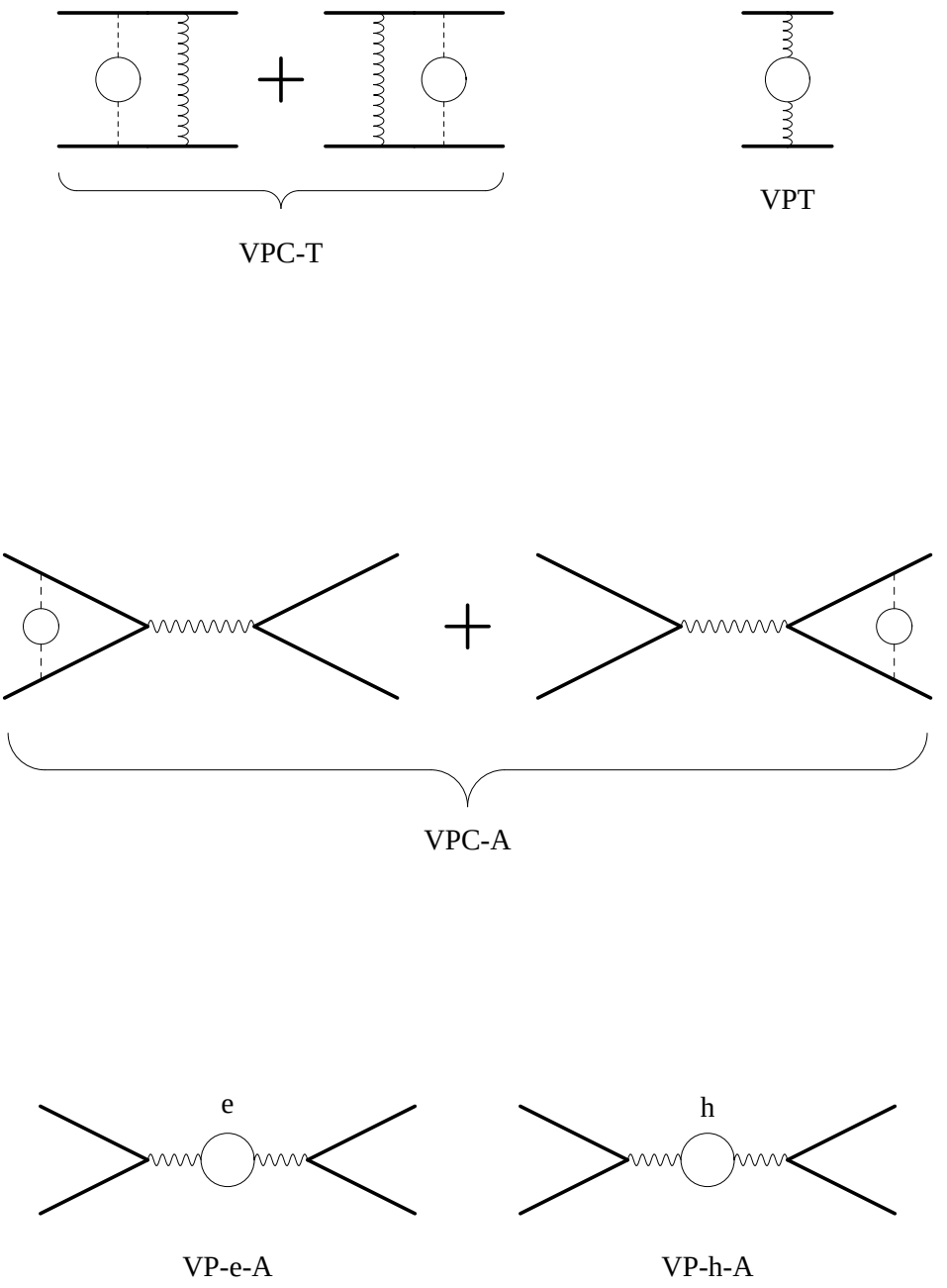

FIG. 5. Corrections of order $\alpha/\pi\, E_F$ to the hyperfine splitting specific to the dimuonic atom. Diagrams are further explained in the text.

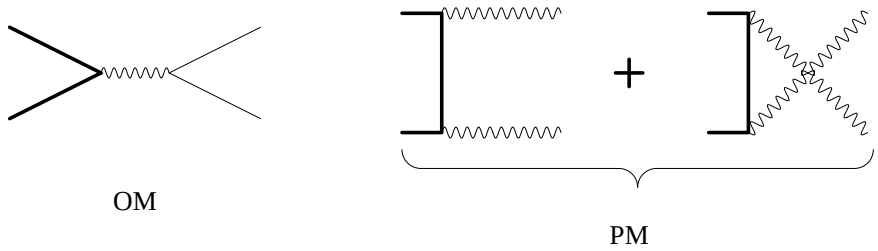

FIG. 6. Decay channels of orthodimuonium (one–photon decay into an electron positron pair, OM) and paradimuonium (two photon decay, PM). The decay channels depicted yield the main contribution to the decay of the system (Γ of order $\alpha^5\, m_\mu$). Bold fermionic lines denote muons, thin lines denote electrons and positrons.

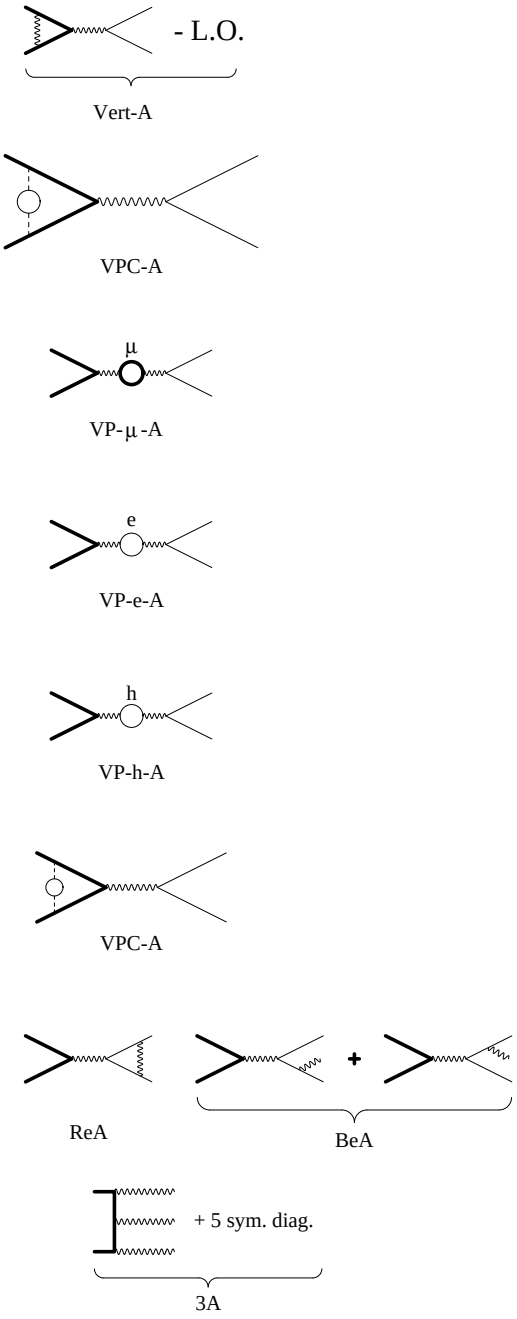

FIG. 7. Order α/π corrections to the decay channels of orthodimuonium. The 5 symmetrical diagrams originate from the symmetrization of photon wave functions.

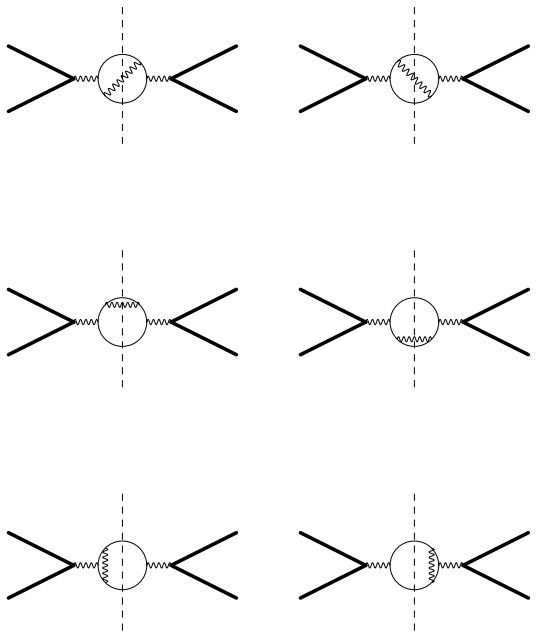

FIG. 8. Evaluation of bremsstrahlung and electron vertex corrections to orthodimuonium decay as imaginary part of the two–loop vacuum polarization insertion in the photon line.

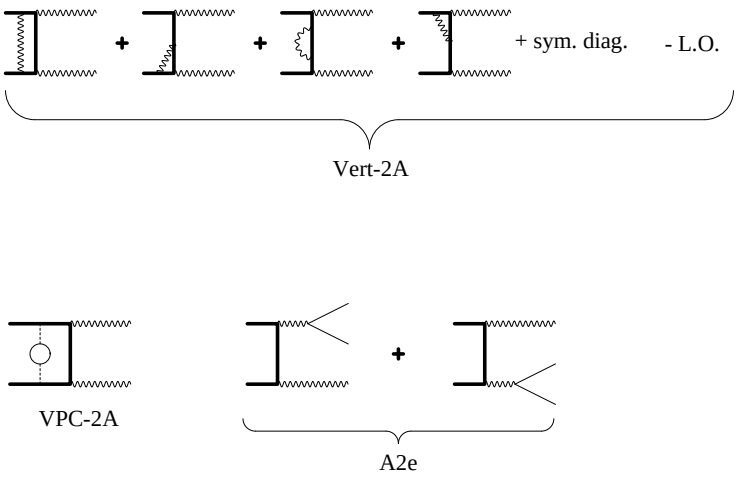

FIG. 9. Order α/π corrections to the decay channels of paradimuonium. The symmetrical diagrams originate from the symmetrization of the photon wave functions.

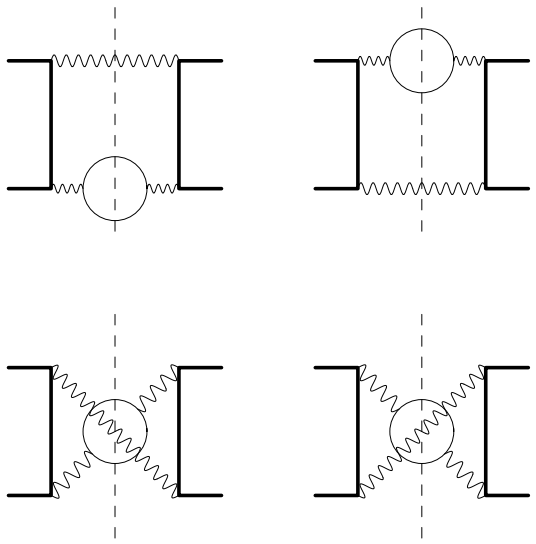

FIG. 10. Evaluation of corrections to the paradimuonium decay caused by the production of an electron positron pair (A2e correction).